frontiers | Frontiers in Physics

TYPE Original Research
PUBLISHED 04 January 2023
DOI 10.3389/fphy.2022.1079641

OPEN ACCESS

EDITED BY
Kh S. Mekheimer,
Al-Azhar University, Egypt

REVIEWED BY
Nehad Ali Shah,
Sejong University, South Korea
M. Sankar,
University of Technology and Applied Sciences (Oman), Oman

*CORRESPONDENCE
Arshad Riaz,
arshad-riaz@ue.edu.pk

SPECIALTY SECTION
This article was submitted to Statistical and Computational Physics, a section of the journal Frontiers in Physics

RECEIVED 25 October 2022
ACCEPTED 05 December 2022
PUBLISHED 04 January 2023

CITATION
Bilal S, Khan NZ, Fatima I, Riaz A, Ansari GJ, Alhazmi SE and El-Din EMT (2023), Mixed convective heat transfer in a power-law fluid in a square enclosure: Higher order finite element solutions. *Front. Phys.* 10:1079641. doi: 10.3389/fphy.2022.1079641

RETRACTED: Mixed convective heat transfer in a power-law fluid in a square enclosure: Higher order finite element solutions

S. Bilal[1], Noor Zeb Khan[1], Iqra Fatima[1], Arshad Riaz[2]*, Ghulam Jillani Ansari[3], Sharifah E. Alhazmi[4] and ElSayed M. Tag El-Din[5]

[1]Department of Mathematics, Air University, Islamabad, Pakistan, [2]Department of Mathematics, Division of Science and Technology, University of Education, Lahore, Pakistan, [3]Department of Information Sciences, Division of Science and Technology, University of Education, Lahore, Pakistan, [4]Mathematics Department, Al-Qunfudah University College, Umm Al-Qura University, Mecca, Saudi Arabia, [5]Center of Research, Faculty of Engineering, Future University in Egypt, New Cairo, Egypt

Incorporation of momentum gradients produced due to inertial motion of the lid along with the presence of temperature differences in the configuration make the physical problem more significant. The joint variation of momentum and thermal diffusion in diversified natural liquids is recognized as mixed convection. Valuable attention has been received by such a phenomenon in different areas of science and technology such as in wind current–based solar receivers, electronic instruments, control of emergency shutdown in reactors, thermal exchangers, oceanic currents, control of atmospheric pollution, and so on. So, the main focus is to contemplate hydrothermal characteristics of a power-law fluid contained in a square cavity with the movement of the upper lid and being thermally adiabatic. The other extremities are considered to be at rest, and the base wall is prescribed with uniform/non-uniform temperature distributions. The governing formulation of the problem is handled by executing a finite element approach. Hybrid meshing is performed for domain discretization, and weak variational formulation is utilized for formulation discretization. Second-degree polynomials are employed as the interpolation function, providing information about velocity and temperature distributions at boundary and intermediate nodes. The system of finalized non-linear equations is resolved by using the Paradiso software. The results for velocity and temperature distributions are attained comparatively for uniformly and non-uniformly heated profiles. The kinetic energy and average Nusselt number are also computed against flow concerning variables. From the attained graphical and tabular data, it is deduced that by increasing the Reynolds number, inertial forces dominate over buoyancy forces and the effect of lid movement is prominent on flow characteristics. It is also inferred that for the shear thickening case and for all values of the Reynolds number, the average Nusselt number shows a constant behavior.

KEYWORDS

mixed convection, square cavity, uniform/non-uniform heating, finite element method, heat transfer

1 Introduction

Buoyancy- and lid-driven flows inside confined geometries have appealed the promising intent of researchers. Representative fields of interest include flash drying, liquid fuels combustion, food processing plants, evaporation of cyclones, crystal growth, material separation processes, and so on. In recent years, modern technologies demand for combined (buoyancy- and lid-driven) diffusions in different procedures. Considerable work has been published on natural convection describing the role of buoyancy forces. Unfortunately, the combination of free and forced convection seldom arise in practice. Some already published work from where the motivation for the current effort has been taken is described here. Like, Lyican et al. [1] performed numerical computations to interpret hydrothermal characteristics of the natural convective flow in a trapezoidal enclosure by considering adiabatic extremities. Roy and Basak [2] made an outstanding effort to examine heat transfer generated by the thermally driven viscous liquid with a prescription of uniform heat distribution. By measuring the influence of oscillation of the flow and temperature propagation, the dual convective flow of a viscous liquid with wavy boundaries was manifested by Amiri et al. [3]. The impression of permeability on natural convection generated in trapezium along with the production of thermal convective potential with cold and heat parallel boundaries was explicated by Varol et al. [4, 5]. Basak et al. [6] explained flow attributes of the fluid along with heat transfer in different zones of the enclosure by discussing the impact of the flow controlling convection Rayleigh number on momentum and temperature distributions *via* streamlines

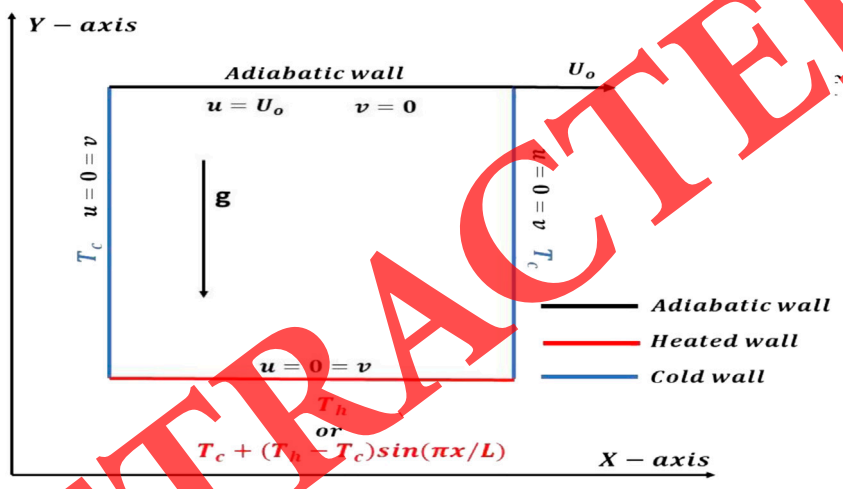

FIGURE 1
Visualization of the enclosure with boundary constraints.

TABLE 1 Mesh statistics at different refinement levels.

Refinement level	#E	DOF	Triangle	Quad	Edge element
Extremely coarse	192	580	128	64	32
Extra coarse	342	976	246	96	48
Coarser	538	1440	418	120	60
Coarse	1002	2560	818	184	92
Normal	1492	3684	1260	232	116
Fine	2516	5900	2228	288	144
Finer	6636	15124	6020	616	308
Extra fine	16952	37508	15752	1200	600
Extremely fine	26212	56028	25012	1200	600

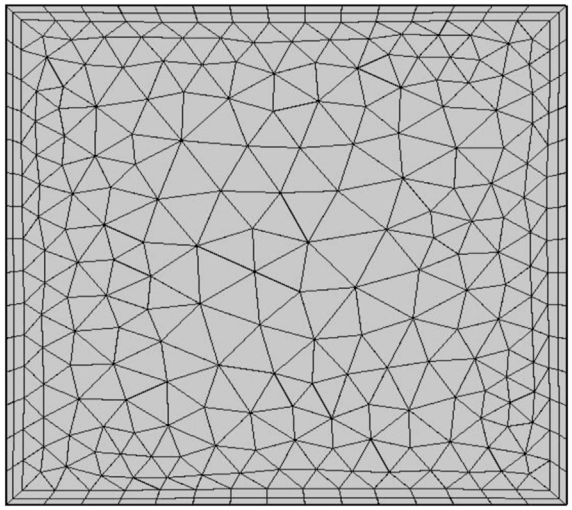

FIGURE 2
Domain discretization at the coarser level.

and isothermal contours, respectively. An innovative approach known as the heat line approach was introduced by Basak [7] to measure free convection in a trapezoidal enclosure. The heat transmission mechanism produced by uniform heat sources at boundaries by implementing the computational approach was addressed by Oztop et al. [8]. Impression of the transverse magnetic field on heat transport in a naturally convective flow of the viscous liquid was engrossed by Mahmoodi and Pour [9]. Convection in the isothermal flow of the viscous liquid saturated in the Darcy medium was accounted by Rehman et al. [10]. Jagadeesha et al. [11, 12] explored the influence of tilt angle formed between sloping sides of the parallelogram cavity on convective transport by measuring flow patterns and thermal fields. They incorporated Darcy's law to depict the impact of permeability on flow and thermal characteristics. Sankar and his coresearchers [13–16] adumbrated convection in the annular region by assuming different physical constraints and by employing a magnetic field and permeability aspects.

Polymeric natured fluids which exhibit both shear thinning and thickening attributes possess marvelous real-world applications. The characterization of such materials is identified by a variation in apparent viscosity against the magnitude of shearing rate. Intuitively, it is verified that coupling of momentum and thermal fields of such liquids in

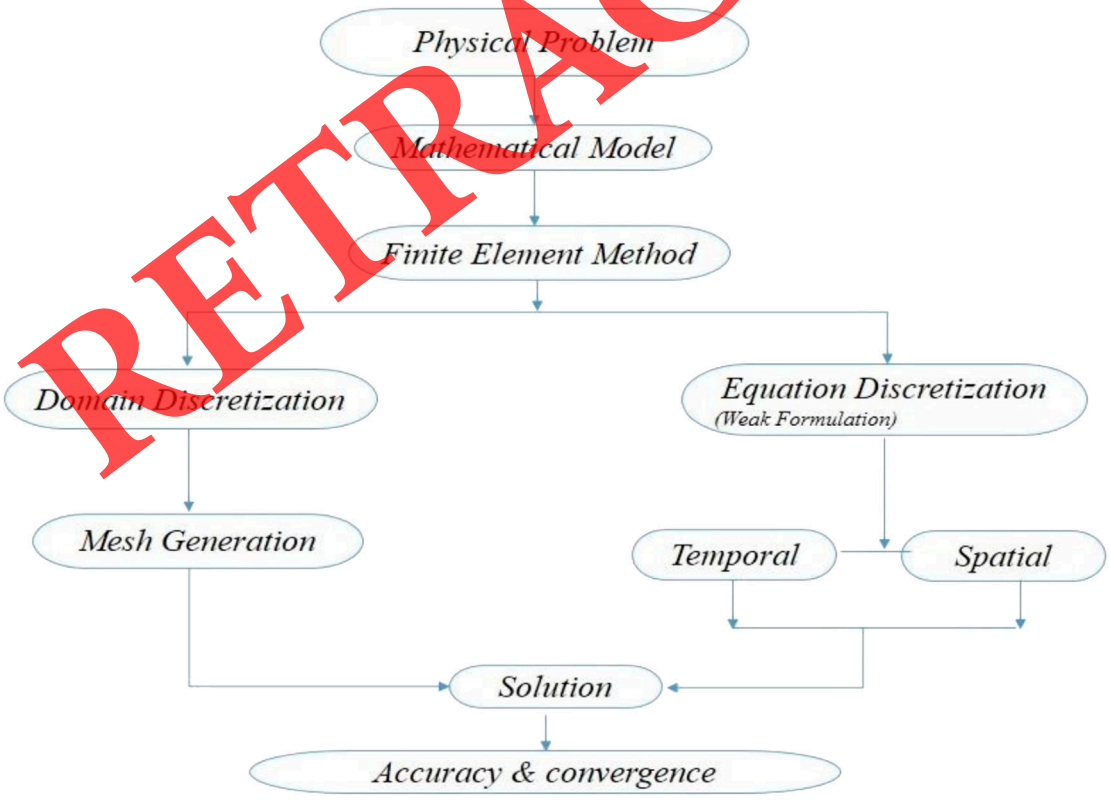

FIGURE 3
Representation of steps in the computational scheme.

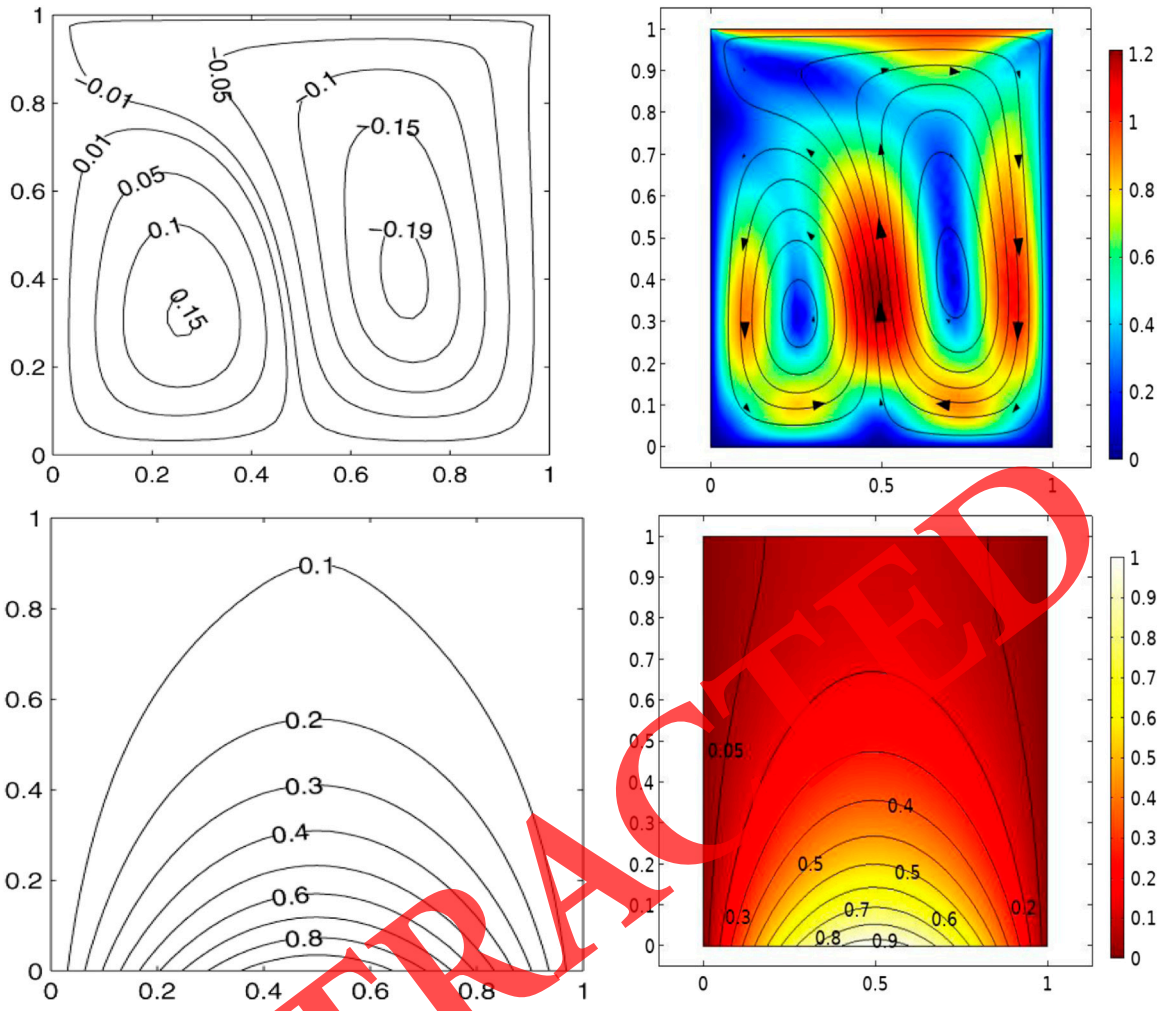

FIGURE 4
Comparison of results with the outcome published by Basak et al. [6].

which viscosity changes point-wise has a more influential role in measuring heat transfer characteristics. Overwhelming fundamental significance of the described situations is found in reduction in heat loss from storage tanks, production of crude oil, reheating of food items, cooling of electronic components, melting and heating of polymeric pallets, and so forth. For a comprehensive mathematical disquisition of the mentioned materials, an outstanding mathematical model renowned as the power-law model is formulated. This model predicts the behavior of polymeric materials at zero and infinite stresses and describes the response of deformation rate. A number of studies pertaining to the power-law material in confined geometries with natural convection have been discussed. For instance, the impact of the Prandtl number and model parameter on thermal diffusion in the fluid along with a change in heat flux was presented by Hartnett [17]. Khezzar et al. [18] demonstrated characteristics of the power-law fluid with impersistent density by utilizing the Boussinesq approximation in a 2D cavity against the Rayleigh number. Sairamu and Chhabra [19] considered the quiescent power-law fluid embedded in a laminar flow enclosed in an inclined enclosure along with temperature-dependent density over a range of kinematic conditions. Mishra and Chhabra [20] executed analysis on a laminar convective flow of the power-law liquid with differentially heated horizontal cylinders aligned in the tandem direction. Some recent developments on non-Newtonian fluids with multiple physical aspects and in different flow generating domains are collected in Refs. [21–25].

Based on thorough review about the related literature, it is explored that studies about the convectively driven flow in

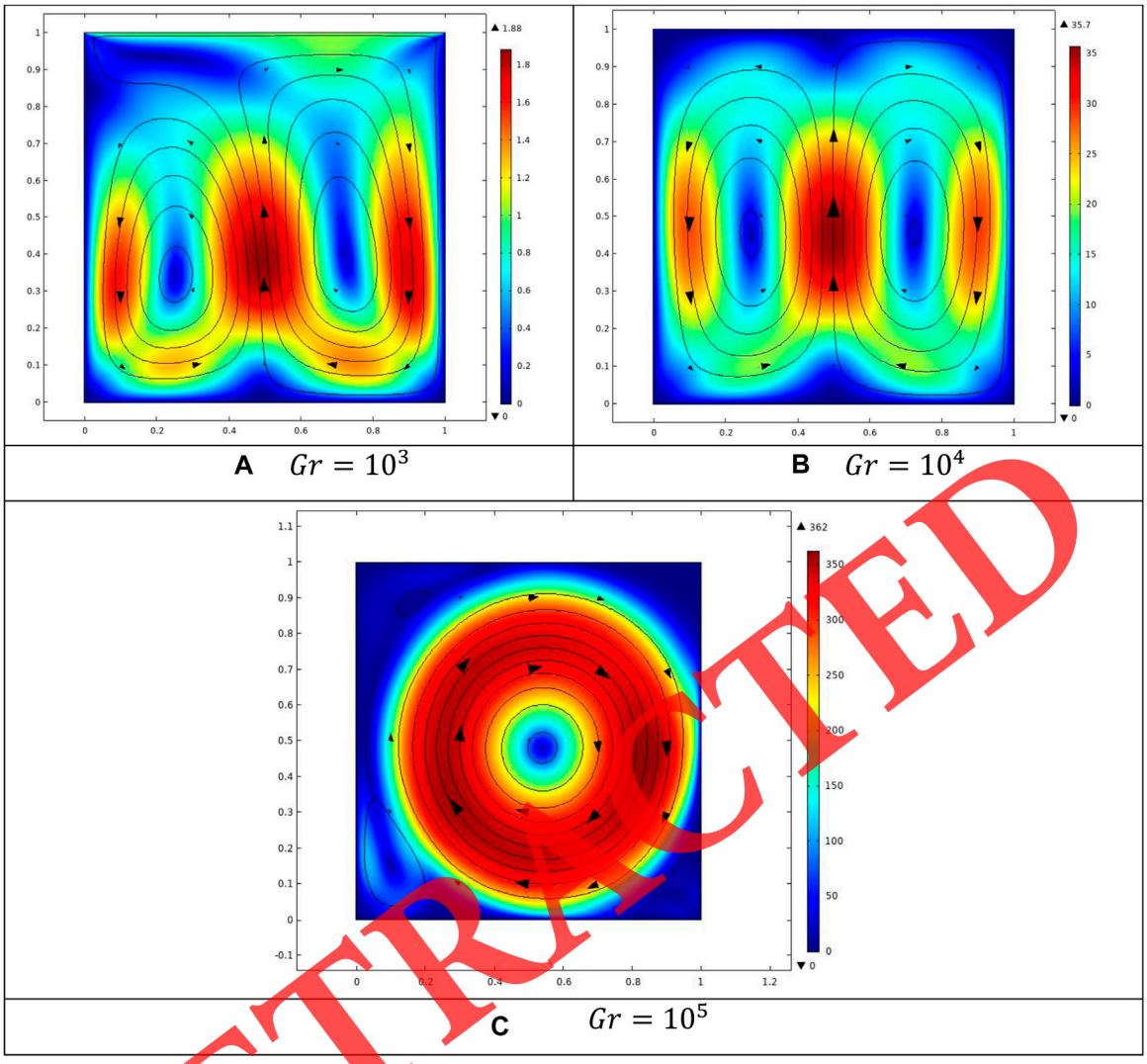

FIGURE 5
Influence of *Gr* on streamlines for the uniform heated case: **(A)** $Gr = 10^3$, **(B)** $Gr = 10^4$, and **(C)** $Gr = 10^5$.

different configurations are abundantly available. But as far as the analysis of joint forced and free convection is concerned, especially in case of non-viscous fluid has not been done yet. So, to fill this gap, the present work is communicated and two additional thermal distributions are entertained in a comparative manner. So, to achieve this task, governing equations are structured in view of PDEs, and afterward, a finite element scheme is opted to simulate results and interpret the influence of the flow concerning on associated profiles. To the best of the authors' knowledge, they have hoped that this work will fill the mentioned gap.

2 Mathematical modeling

The schematic representation of domain characterizing hydrothermal attributes of the power-law fluid enclosed in a square cavity is displayed in Figure 1. Temperature-dependent density is assumed by incorporating the Boussinesq approximation. Shear thinning and thickening aspects of the power-law fluid against different magnitudes of the model parameter are investigated for uniformly and non-uniformly distributed thermal distribution.

The governing equations describing the tensorial representation of the power law are as follows. [6]:

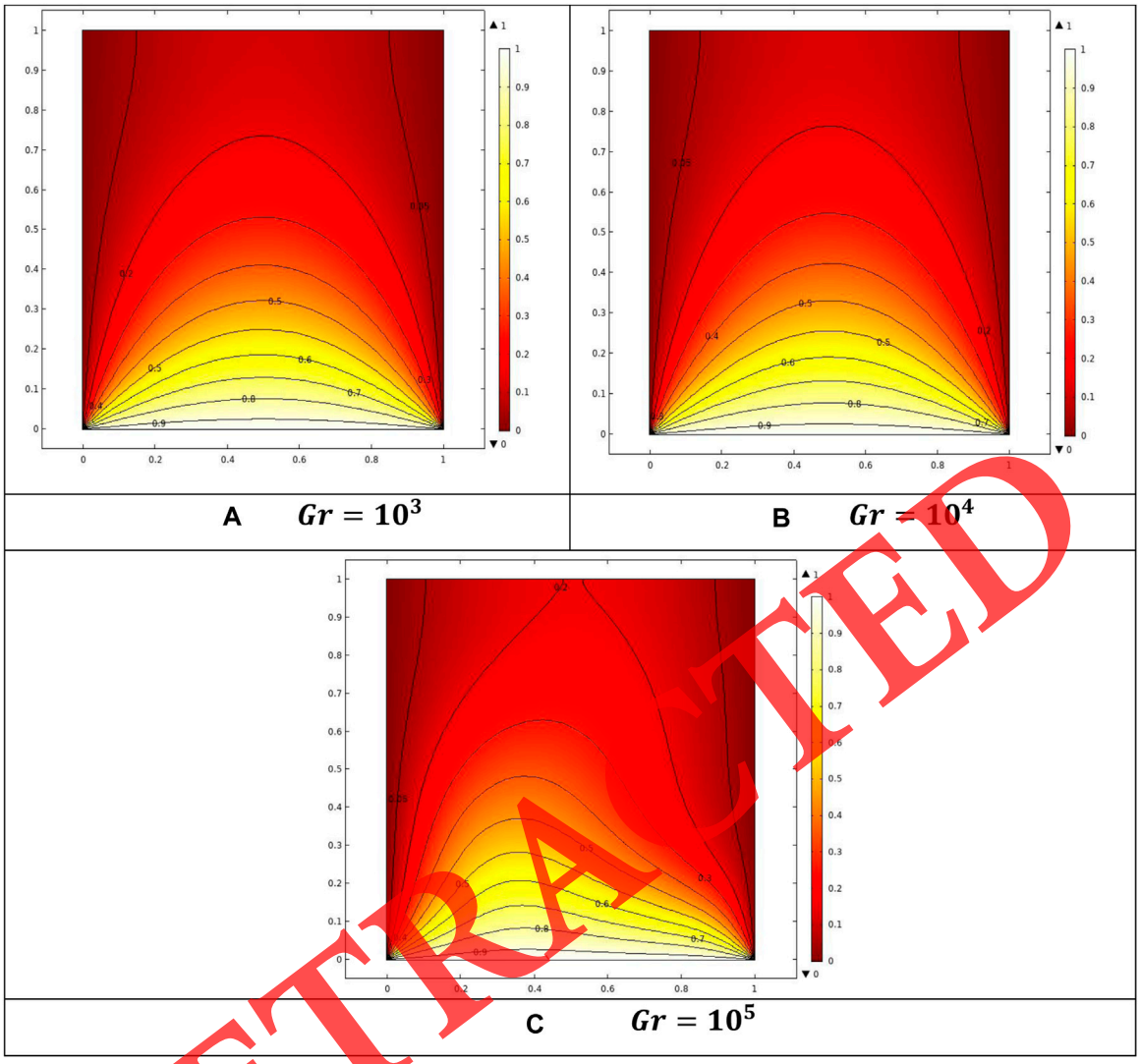

FIGURE 6
Influence of *Gr* on temperature distribution for the uniform heating case: **(A)** $Gr = 10^3$, **(B)** $Gr = 10^4$, and **(C)** $Gr = 10^5$.

$$\frac{\partial u}{\partial x} + \frac{\partial v}{\partial y} = 0 \tag{1}$$

$$uu_x + vu_y = -\frac{1}{\rho}p_x + \left[(\tau_{xx})_x + \left(\tau_{yx}\right)\right] \tag{2}$$

$$uv_x + vv_y = -\frac{1}{\rho}\mathrm{p}_y + \left[\left(\tau_{xy}\right)_x + \left(\tau_{yy}\right)_y\right] + g\beta(T - T_C) \tag{3}$$

$$\tau_{ij} = 2\mu D_{ij} = 2\mu\left((u_i)_{x_j} + \left(u_j\right)_{x_i}\right) \tag{4}$$

$$\mu = m\left[2\left((u_x)^2 + \left(v_y\right)^2\right) + \left(v_x + u_y\right)^2\right]^{\frac{(n-1)}{2}} \tag{5}$$

$$\rho C_p\left(uT_x + vT_y\right) = k\left(T_{xx} + T_{yy}\right) \tag{6}$$

Associated boundary constraints are as follows:

$$u(x, L) = 1 \tag{7}$$

at the top horizontal wall; $u(x,0) = u(0,y) = u(L,y) = 0 = v(x,0) = v(x,L) = v(0,Y) = v(L,y)$ at other walls; $T(x,0) = 1$ or $T(x,0) = sin(\frac{\pi x}{L})$ at the bottom horizontal wall;

$$T(0, y) = 0 = T(L, y) \tag{8}$$

at the side vertical walls; and $T_y(x, L) = 0$ at the top horizontal wall.

The defined equations in Eqs. 2–4 are dimensionalized by the mentioned transformation

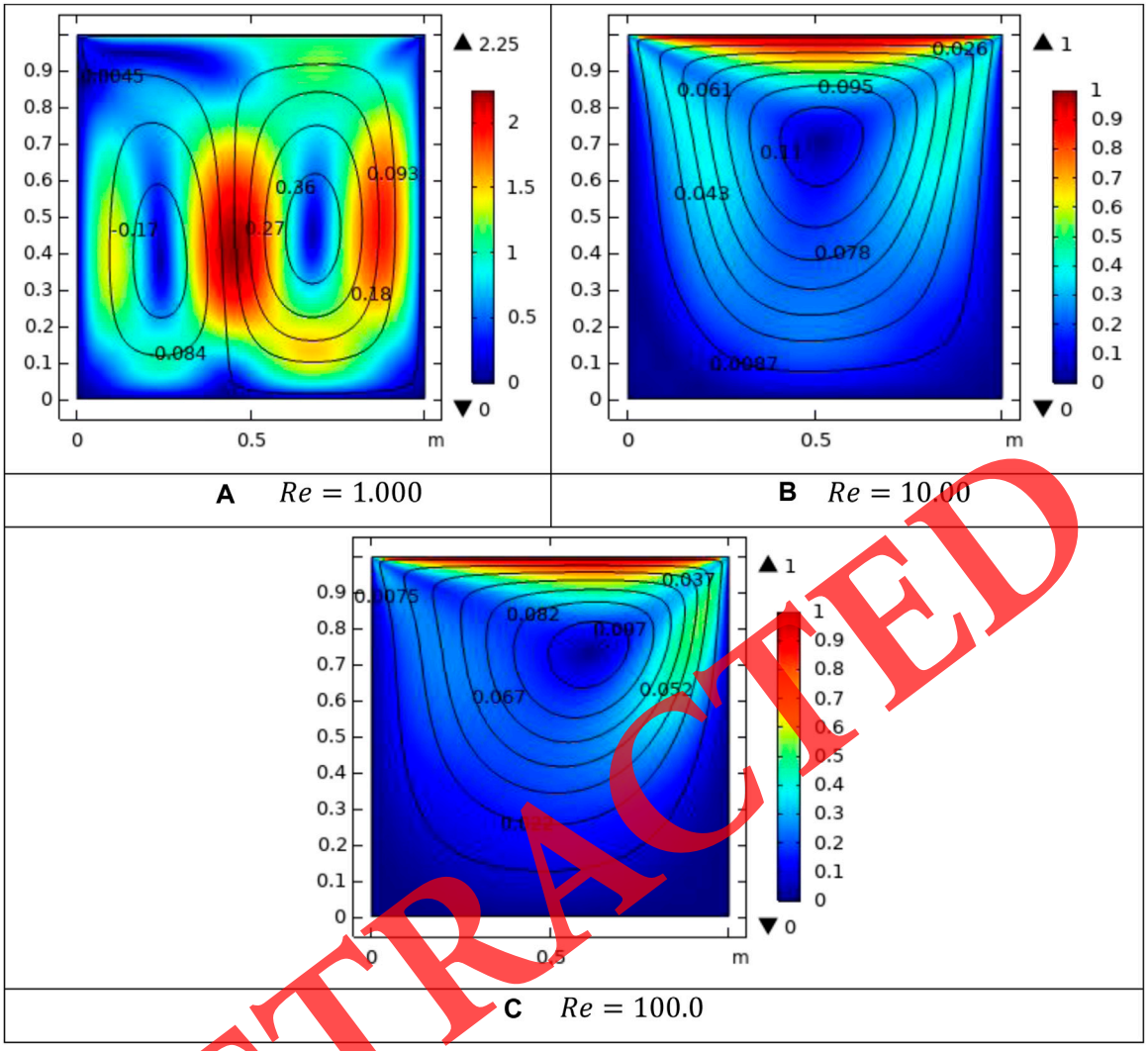

FIGURE 7
Influence of *Re* on streamlines for the uniform heating case: **(A)** *Re* = 1.000, **(B)** *Re* = 10.00, and **(C)** *Re* = 100.0.

$$X^{\star} = \frac{x}{L},\ Y^{\star} = \frac{y}{L},\ u^{\star} = \frac{u}{U},\ v^{\star} = \frac{v}{U},\ \theta^{\star} = \frac{T - T_C}{T_h - T_c},\ \text{and}\ P^{\star} = \frac{P}{\rho U^2} \tag{9}$$

$$\mu = \left(\frac{U}{L}\right)^{n-1} \mu^{\star}.$$

Eqs. 1–10 are reduced to non-dimensionalized representation

$$u^{\star}_{X^{\star}} + v^{\star}_{Y^{\star}} = 0 \tag{10}$$

$$u^{\star}u^{\star}_{X^{\star}} + v^{\star}u^{\star}_{Y^{\star}} = -P^{\star}_{X^{\star}} + \frac{1}{\mathrm{Re}}\left[2\frac{\partial}{\partial X^{\star}}\left(\frac{\mu^{\star}}{m}u^{\star}_{X^{\star}}\right) + \frac{\partial}{\partial Y^{\star}}\left\{\frac{\mu^{\star}}{m}\left(u^{\star}_{Y^{\star}} + v^{\star}_{X^{\star}}\right)\right\}\right] \tag{11}$$

$$u^{\star}v^{\star}_{X^{\star}} + v^{\star}v^{\star}_{Y^{\star}} = -P^{\star}_{Y^{\star}} + \frac{1}{\mathrm{Re}}\left[2\frac{\partial}{\partial Y^{\star}}\left\{\frac{\mu^{\star}}{m}\left(v^{\star}_{Y^{\star}}\right)\right\} + \frac{\partial}{\partial X^{\star}}\left\{\mu^{\star}\left(u^{\star}_{Y^{\star}} + v^{\star}_{X^{\star}}\right)\right\}\right] + \frac{Gr}{\mathrm{Re}^2}\theta^{\star} \tag{12}$$

$$u^{\star}\theta^{\star}_{X^{\star}} + v^{\star}\theta^{\star}_{Y^{\star}} = \frac{1}{\mathrm{PrRe}}\left(\theta^{\star}_{X^{\star}X^{\star}} + \theta^{\star}_{Y^{\star}Y^{\star}}\right). \tag{13}$$

Boundary constraints in a dimensionless form are given as follows:
$u^{\star}(X^{\star}, 1) = 1$ at the top horizontal wall;

$$u^{\star}(X^{\star}, 0) = u^{\star}(0, Y^{\star}) = u^{\star}(1, Y^{\star}) = 0 = v^{\star}(X^{\star}, 0) = v^{\star}(X^{\star}, 1) = v^{\star}(0, Y^{\star}) = v^{\star}(1, Y^{\star}) \tag{14}$$

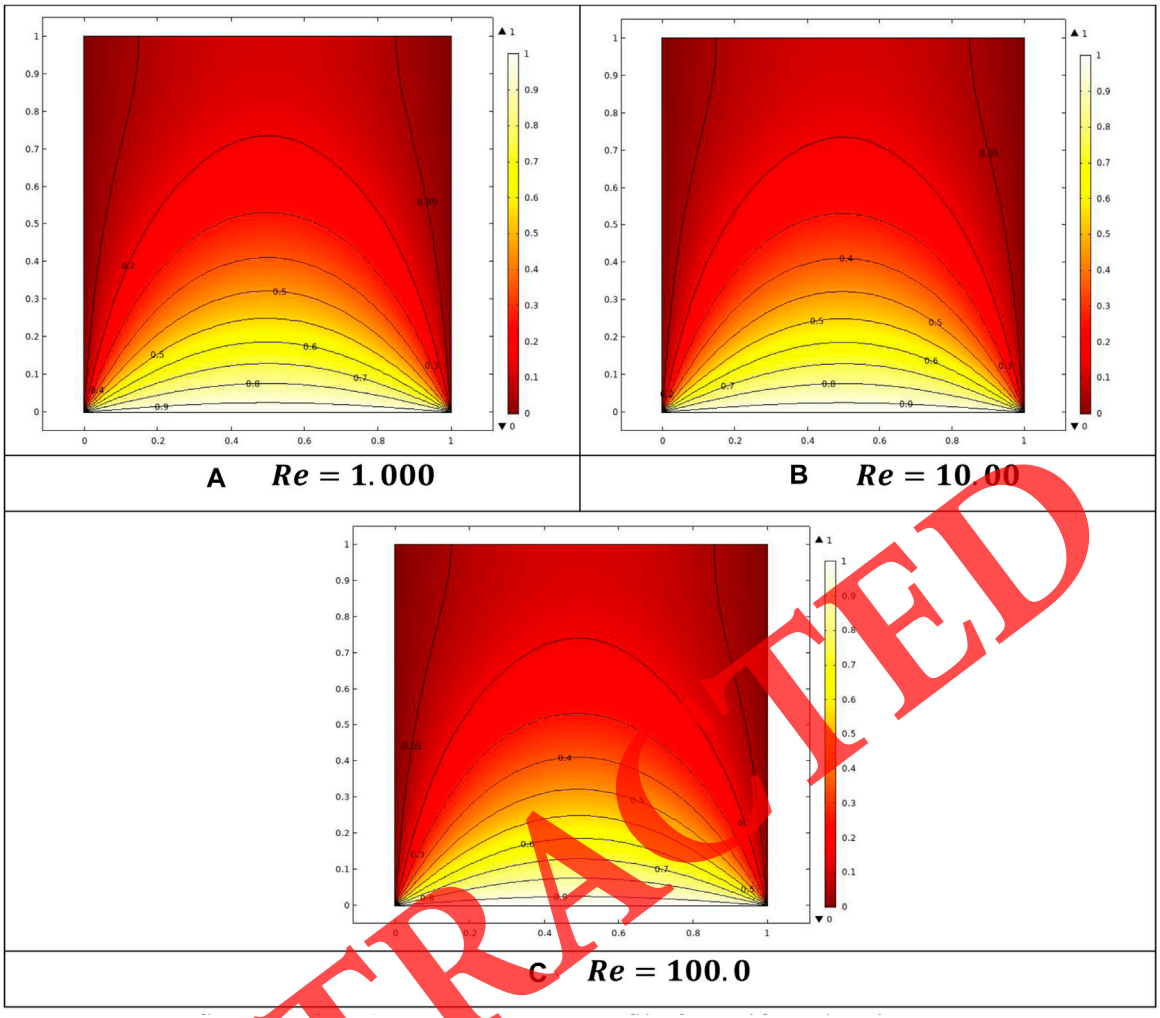

FIGURE 8
Influence of *Re* on the temperature profile for the uniform heating case: **(A)** *Re* = 1.000, **(B)** *Re* = 10.00, and **(C)** *Re* = 100.0.

at all the solid walls; $\theta^*(X^*, 0) = 1$ or $\theta^*(X^*, 0) = \sin(\pi X^*)$ at the bottom horizontal wall;

$$\theta^*(0, Y^*) = 0 = \theta^*(1, Y^*) \tag{15}$$

at the side vertical walls; And $\theta^*_{Y^*}(Y^*, 1) = 0$ at the top horizontal wall.

The involved physical variables in the analysis are represented as follows:

$$Re = \frac{U_{Lid}\, L}{\nu},\ Gr = \frac{g\beta(T_h - T_c)L^3}{\nu^2} \text{ and } \Pr = \frac{\nu}{\alpha}. \tag{16}$$

Global quantity of interest named as the Nusselt number is also computed as follows:

$$Nu = \left.\frac{\partial\theta}{\partial n}\right|_{wall} \text{ and } Nu_{avg} = \frac{1}{L}\int_0^L Nu dS. \tag{17}$$

3 Computational procedure

Analytical methods are unable to solve the resultant model differential equations attained for complex engineering problems, especially in view of the mixed convection problem discussed in the current study that contains non-linear complexity in both momentum and temperature equations. In addition, singularity is also generated at the boundary of the domain. So, execution of computational approaches such as finite

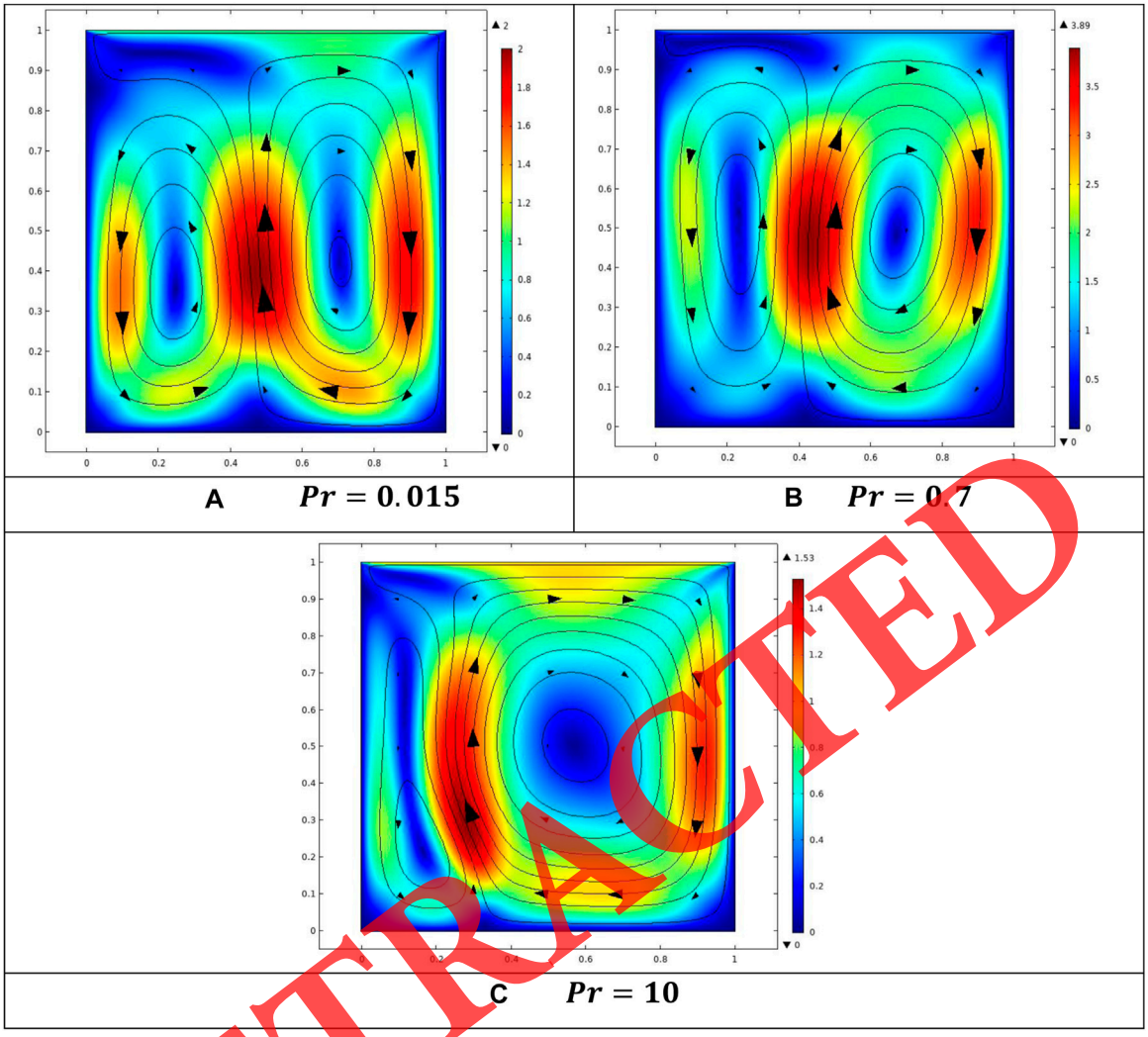

FIGURE 9
Influence of *Pr* on streamlines for the uniform heating case: **(A)** *Pr* = 0.015, **(B)** *Pr* = 0.7, and **(C)** *Pr* = 10.

volume, finite element, and finite difference are considered to be the fittest to attain the approximate solution [26–29]. Among this, the most flexible and rapid technique is the finite element scheme. To resolve the complexly structured problem first, discretization of the domain is performed by executing hp-refinement. Since the current problem is in 2D, the completed domain is distributed in the form triangular and rectangular elements as shown in Figure 2 and Table 1. Afterward, by using the Lagrange interpolation formula shape function, defining the behavior of field variables at each node is obliged. Here, the quadratic shape function consisting of piece-wise continuous second-degree polynomial for velocity and temperature is opted, whereas pressure is approximated by linear polynomial. After the selection of suitable shape functions, discretization of the governing differential system by employing a weak formulation variational procedure is capitalized and element level equations are formed. With the help of the decided shape function, the construction of basic functions is controlled. Afterward, the associated boundary conditions are loaded in the governing equations and the system of non-linear equations is developed. After that, Newton's approach is used to linearize non-linearized expressions, and the resulting linear system of equations is solved directly using an elimination-based method with a unique rearrangement of unknowns. The calculations scheme is shown in Figure 3.

4 Results and interpretation

The effect of flow controlling parameters on velocity and temperature distributions in view of the streamline and isotherm representation is discussed in this portion. Since,

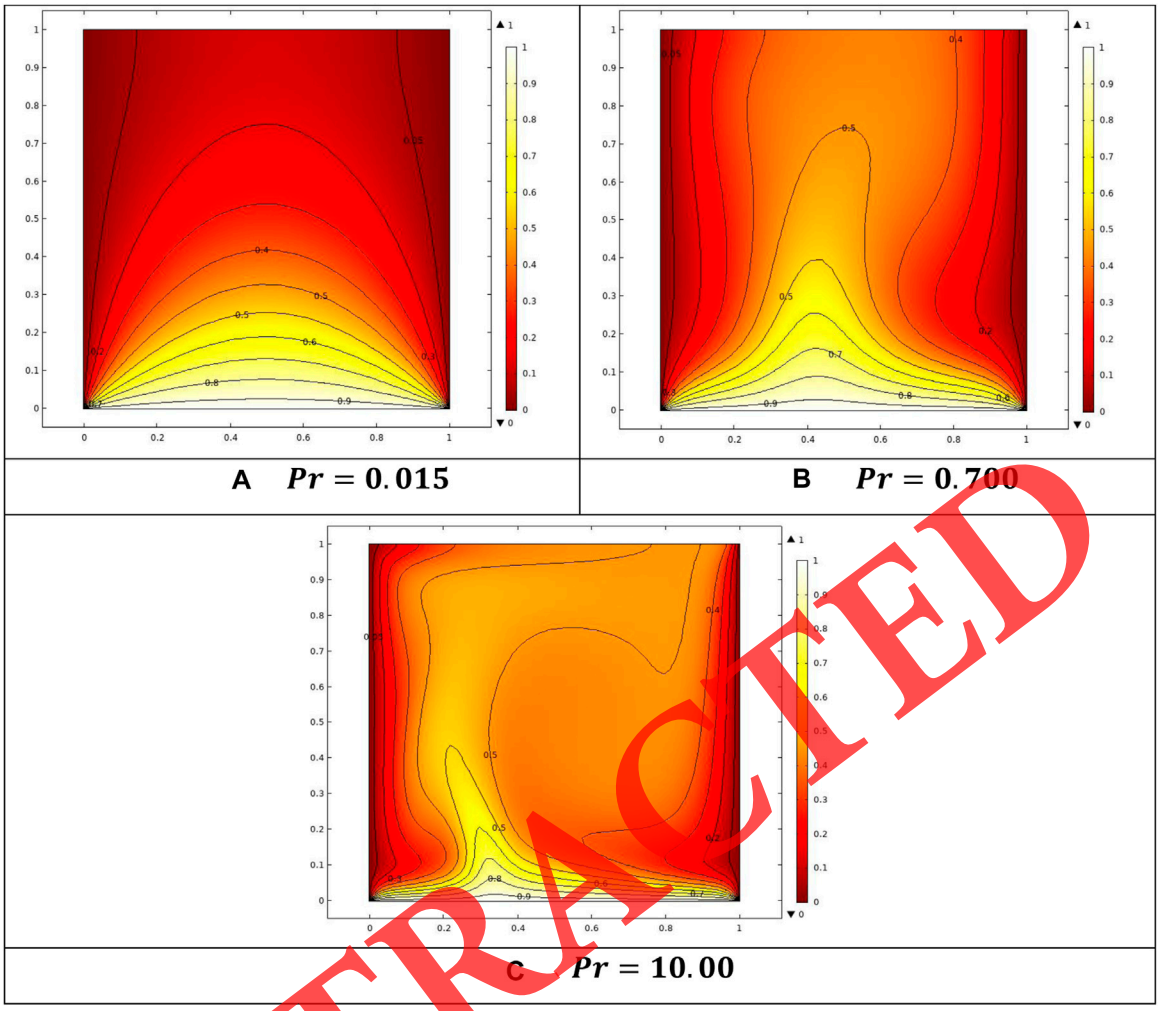

FIGURE 10
Influence of *Pr* on temperature distribution for the uniform heating case: **(A)** *Pr* = 0.015, **(B)** *Pr* = 0.700, and **(C)** *Pr* = 10.00.

in the present problem, a mixed convection is assumed, which is produced by the motion of the upper wall and uniformly/non-uniformly heated base wall, it is analyzed against the Reynolds number (Ra) and Grashof number. In addition, different cases of the power-law index (n) are taken into account which represents shear thinning and thickening properties of the fluid.

4.1 Program validation and comparison test

To assure the accuracy and credibility of the implemented computation scheme, it is validated with results published by Basak et al. [6] by restricting the present problem to a Newtonian case for $n = 1$ as shown in Figure 4. Here, streamlines and isotherms are generated by fixing $Pr = 0.7$, $Re = 1.0$, and $Gr = 10^3$. From the displayed sketches, a complete match of results is seen, which develops the trust of readers to consider the present study as a reference.

The effectiveness of the Grashof number (Gr) on momentum distribution is given by considering vast range varying from 10^3 to 10^5 and providing other parameters with fixed values such as $Pr = 0.015$, $Re = 1.0$, and $n = 0.8$. From the illustrated sketch (in Figures 5A–C), it is noticed that due to the increase in Gr, velocity change in the domain is dependent on buoyancy forces. In addition, Re is assumed to be 1 which shows no influence of inertial forces. It is also observed that at $Gr = 10^3$ and 10^4, two primary vortices are formed in which fluids are moving in clockwise and anti-clock

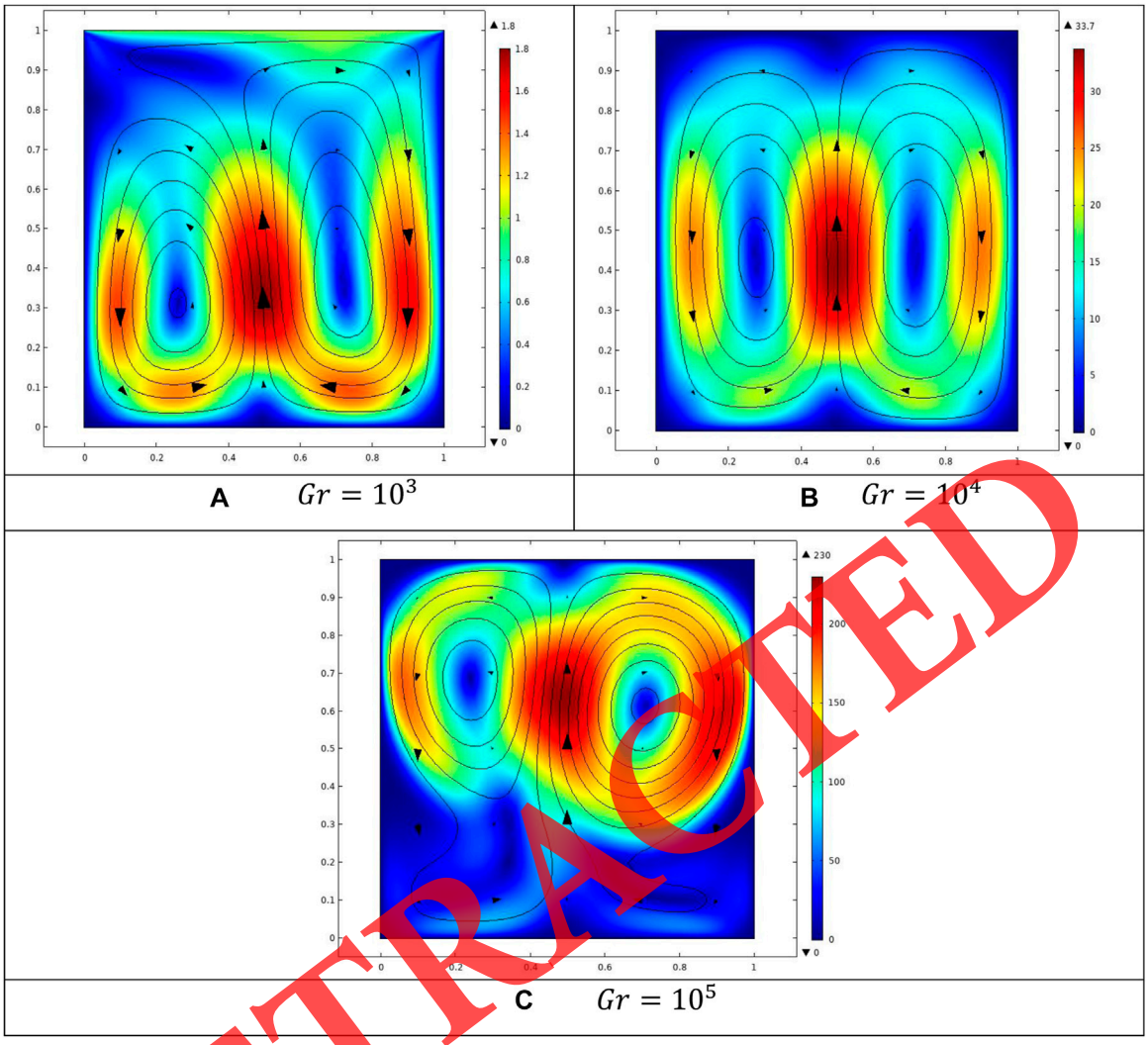

FIGURE 11
Influence of *Gr* on streamlines for the non-uniform heating case: **(A)** $Gr = 10^3$, **(B)** $Gr = 10^4$, and **(C)** $Gr = 10^5$.

wise directions. However, at $Gr = 10^5$, the secondary vortex disappears and the fluid starts moving in a single circular vortex. The reason behind this impact is that by increasing *Gr*, viscosity of the fluid decreases due to which the movement of particles raises, which is evident from the mathematical relation, that is, $Gr = \frac{g\beta(T_h - T_c)L^3}{\nu^2}$.

Change in the temperature profile versus the Grashof number (*Gr*) in view of isothermal patterns is addressed in Figures 6A–C. During the simulations, *Gr* is varied between 10^3 and 10^5 and other concerning parameters are fixed at $Pr = 0.015$, $Re = 1.000$, and $n = 0.8$. An important direction to observe is that in the case of uniform heating, thermal singularity is generated at the left and right most corners of the cavity due to the provision of a uniform heat source. Symmetric aptitude of the isotherm is adhered to in the case of $Gr = 10^3$ and 10^4, whereas the deviation in the pattern is attained at $Gr = 10^5$ in the middle line. The reason behind this behavior is that at $Gr = 10^5$, the production of the temperature gradient exemplifies due to which the transmission of heat from the hotter zone to the colder one increases and the symmetricity is disturbed.

The dominating role of the Reynolds number (*Re*) in controlling lid-driven forces and in managing the phenomenon of mixed convection is explicated in Figures 7A–C. In this sketch, streamlines are represented against variation in (*Re*) from 1 to 100 and with fixation of $Pr = 0.015$ and $Gr = 10^3$. It is seen that at $Re = 1$, the impact of natural convection dominates over forced convection due to

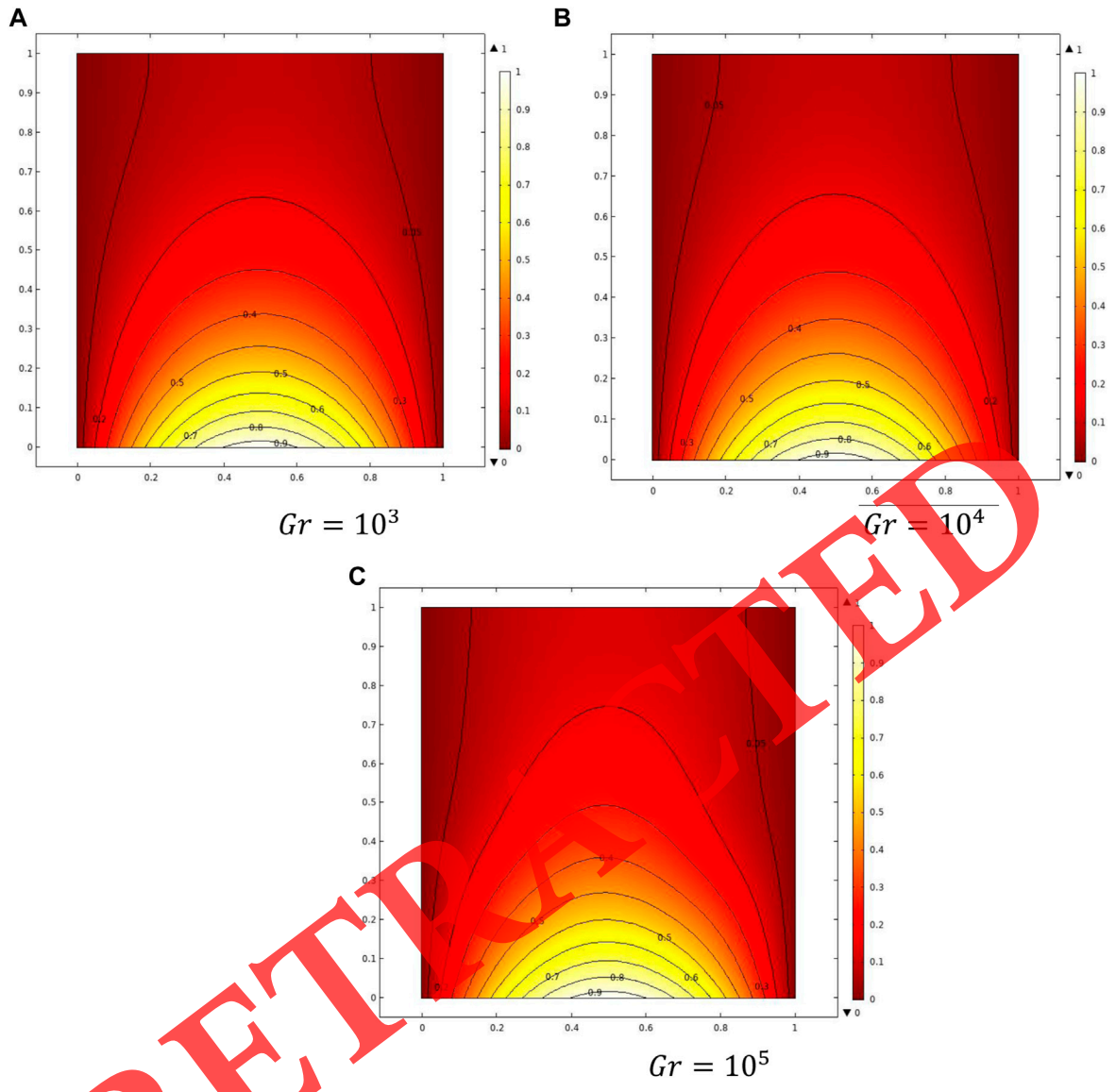

FIGURE 12
Influence of *Gr* on temperature with non-uniform heating: **(A)** $Gr = 10^3$, **(B)** $Gr = 10^4$, and **(C)** $Gr = 10^5$.

which circulations are generated in the flow domain. But by increasing the magnitude of *Re* from 10 to 100, the effectiveness of inertial forces is dominated due to which the movement of the fluid near the upper lid is generated. Maximum velocity of the fluid is attained near the upper wall due to the movement of the wall and only primary vortex are generated. In the case of $Re = 100$, the role of inertial forces dominates over buoyancy forces due to which again a similar trend is observed as in the case of $Re = 10$.

The description of the thermal distribution against the Reynolds number (Re) with $Pr = 0.015$ and $Gr = 10^3$ is evaluated in Figure 8 for uniform heating. No obvious change in isotherms is depicted at each magnitude of *Re*. This justifies the fact that for the production of convection in the domain, the role of the Prandtl number cannot be neglected.

The effect of incrementing magnitude of the Prandtl number (Pr) on velocity distribution is seen in Figures 9A–C. Here, $Gr = 10^3$, $Re = 1$, and $n = 0.8$ are managed and the situation of uniform heating is accounted. Since the Prandtl number (Pr) shows the significant ratio of momentum to thermal diffusivities and plays a vital role in diffusion

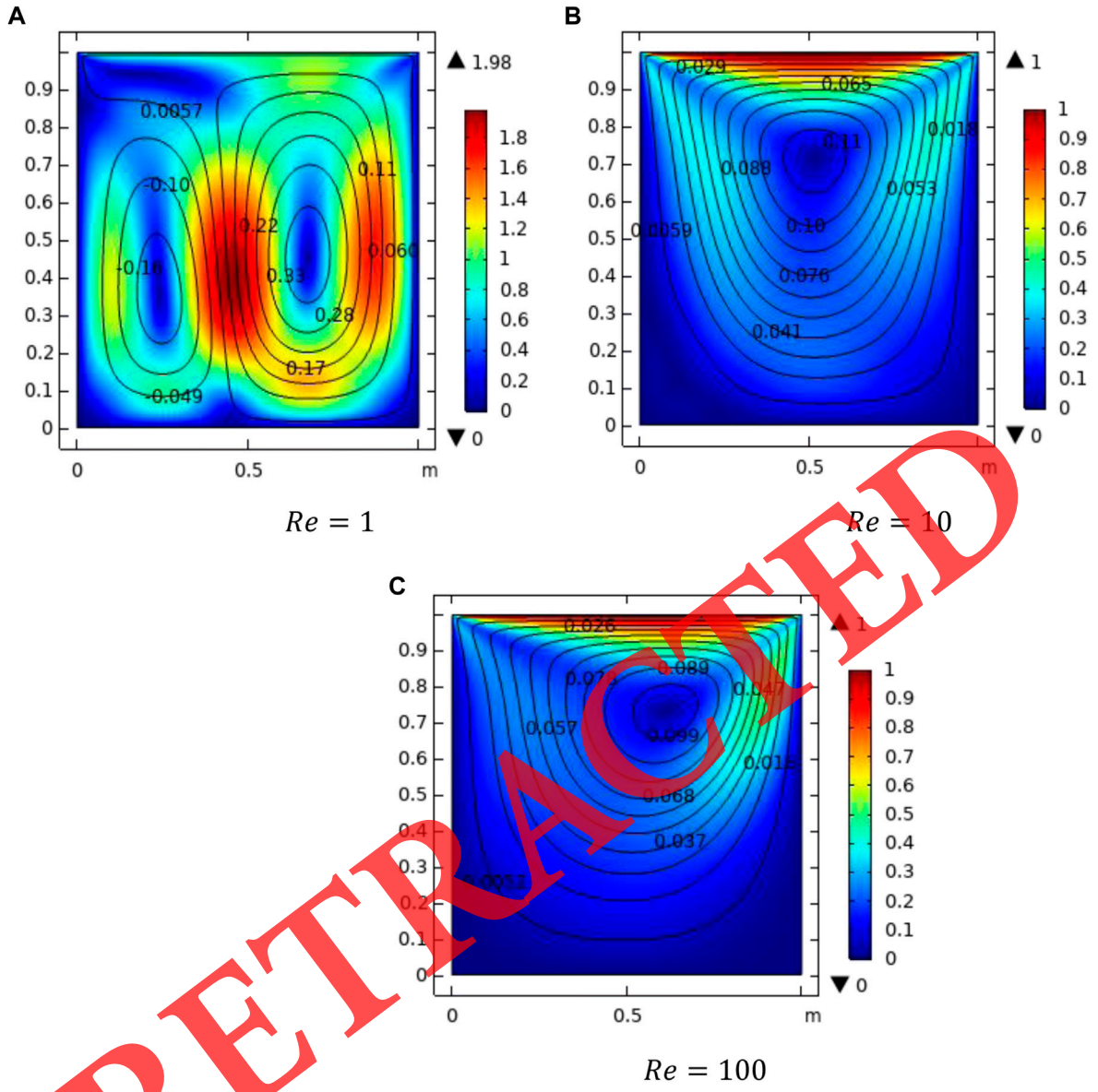

FIGURE 13
Influence of *Re* on streamlines for the non-uniform heating case: **(A)** *Re* = 1, **(B)** *Re* = 10, and **(C)** *Re* = 100.

control, this figure is displayed. From the exhibited graphs, it is observed that vortices squeeze at *Pr* = 10 due to the huge production of momentum diffusivity.

Discussion about the impact of Pr on the thermal profile for uniform heat distribution through isothermal plots is addressed in Figures 10A–C. It is revealed that symmetricity of lines is immensely disturbed when the Prandtl number increases from 0.015 to 10. At lower magnitude of Pr, that is, at 0.015, the thermal diffusion is maximum and heat generated from the bottom wall due to uniform heat supply. In addition, it is seen that the magnitude of heat transferred in the case of *Pr* = 10 is more due to uplift in momentum diffusivity, due to which the kinetic energy of particles increases. Attachment of isotherms with boundaries is seen at a larger magnitude of *Pr*.

The velocity distribution in assistance with the streamline pattern against the Grashof number (Gr) is probed in Figures 11A–C. A wide range of *Gr* is selected from 10^3 to 10^5, *Re* is fixed at 1, and the power-law index (n) is kept constant at 0.5. Unlike the variation in the velocity profile against *Gr* in the

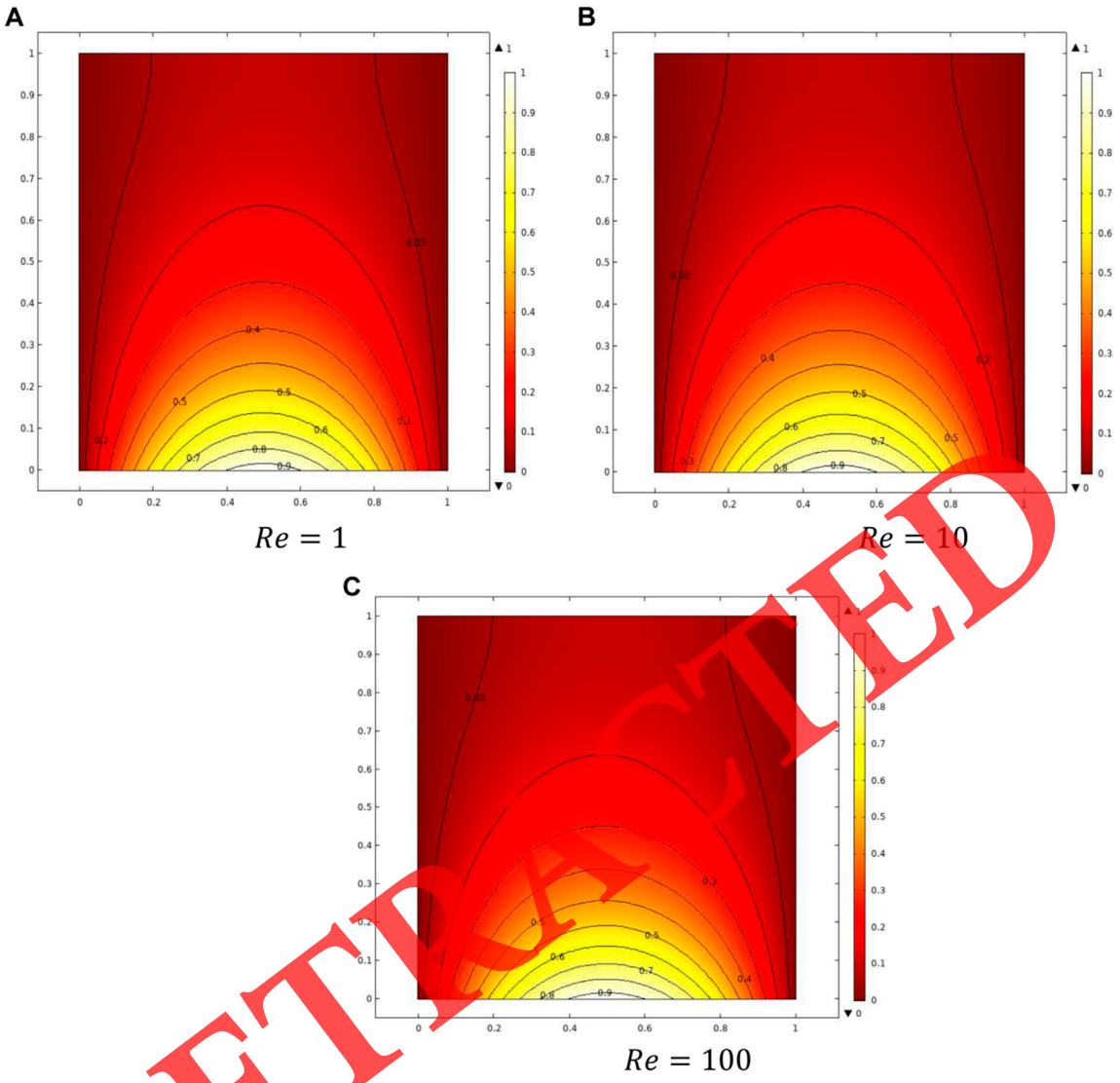

FIGURE 14
Influence of Re on the temperature profile for the non-uniform heating case. **(A)** $Re = 1$, **(B)** $Re = 10$, **(C)** $Re = 100$.

case of uniform heating, here, the behavior is quite different. Here, it is revealed that primary and secondary vortices remain intact and move toward the upper wall. It shows that even at $Re = 1$, the role of inertial forces is also present, which seems to be neglected in the case of uniform heating. It adheres that buoyancy forces are still dominant over inertial forces with an increase in Gr. This fact is proved by the reason that an increment in Gr causes the viscosity to reduce and less resistance will be offered to the molecules.

The temperature distribution against Gr by employing a non-uniform heating situation is evaluated in Figures 12A–C for $Re = 1$, $n = 0.8$, and $Pr = 0.015$. It is found that isotherm intensity is indicated at $Gr = 10^5$, due to the production of thermal convective potential in different zones of the enclosure, which is justified by the deviation in isotherms displayed in the figure. It is also manifested that thermal singularity is removed in the case of non-uniform heating, which is produced in the situation of uniform heating. The perfect parabolic behavior of isotherms is attained at $Gr = 10^3$ and 10^4, which discloses that heat propagated in a parabolic form from the base wall to the upper boundary.

The deviation in velocity distribution against the Reynolds number (Re) is manipulated in Figures 13A–C. During the evaluation of this sketch, three different magnitudes of Re are taken, which shows the dominance of different regimes. At $Re = 1$, the forced and free convection balances each other's effects and

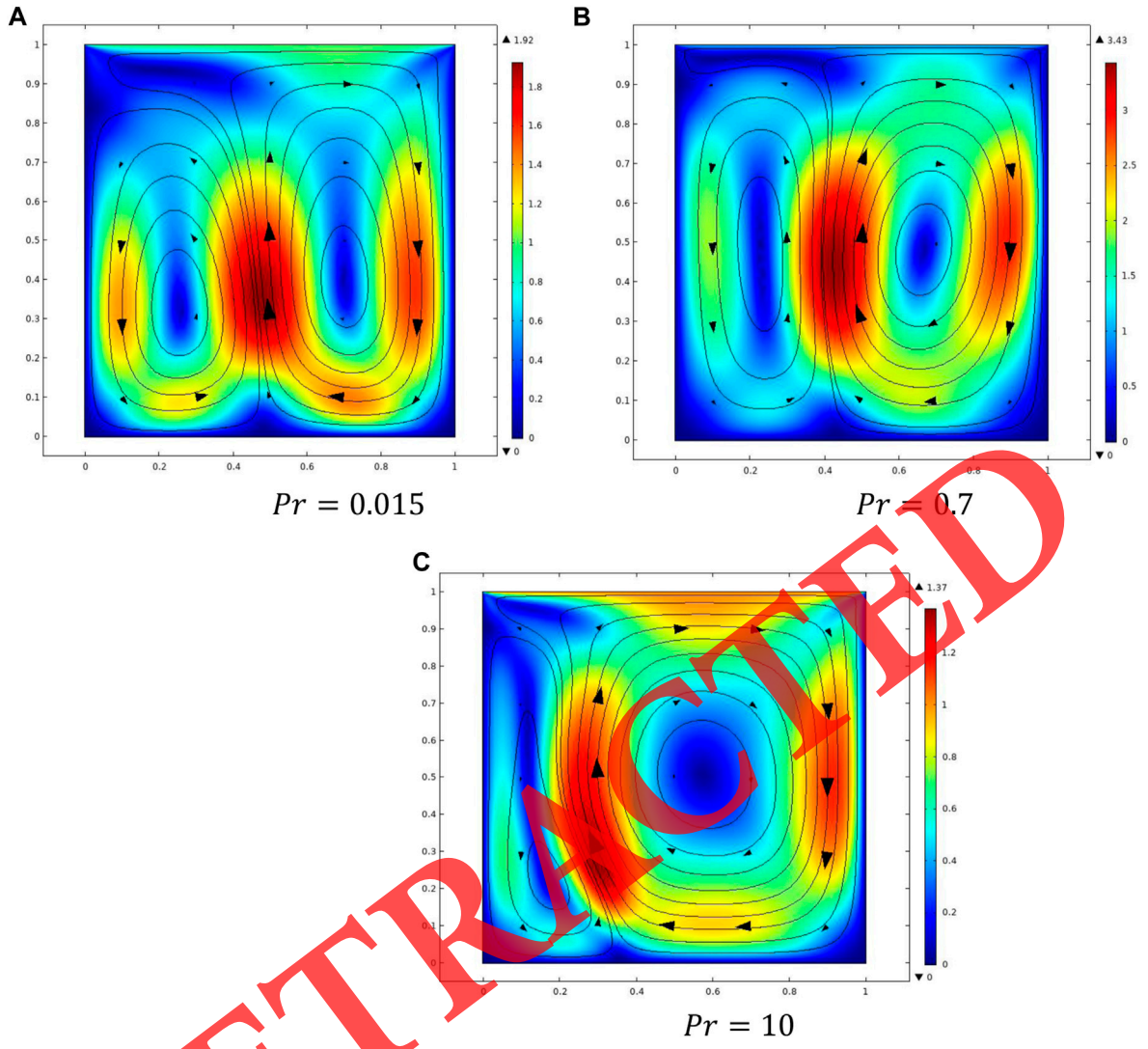

FIGURE 15
Influence of *Pr* on streamlines for the non-uniform heating case: **(A)** *Pr* = 0.015, **(B)** *Pr* = 0.7, and **(C)** *Pr* = 10.

no one dominates the other, whereas at *Re* = 10, the impact of natural convection dominates over forced convection, but in the case of *Re* = 100, forced convection effects on flow characteristics are more than the free convection regime. From the plots, it is seen that maximum velocity in the flow is attained near the moved wall and zero velocity is found where no slip conditions are applied.

No significant change in the temperature distribution evidenced against the Reynolds number (Re) in spite of providing non-uniform heating at the base wall is illustrated in Figures 14A–C. This behavior is similar to the case of uniform heating. This figure shows that consideration of high *Pr* in the case of temperature diffusion is more valuable. Since *Pr* is taken as 0.015 which is much lower in magnitude, no change is observed.

Streamline patterns showing change in the momentum profile against *Pr* is elaborated in Figures 15A–C. It is seen that at *Pr* = 0.015 and 7, two vortices are formed, whereas at *Pr* = 10, the left primary vortex squeezes and merges into the other. It is seen that maximum velocity is attained at a lower magnitude of *Pr* because by increasing *Pr*, viscosity of the fluid increases, due to which viscous force causes the fluid particles to move with less velocity.

Transmission of heat in an enclosure by providing non-uniform heating at the base wall was divulged against *Pr* in

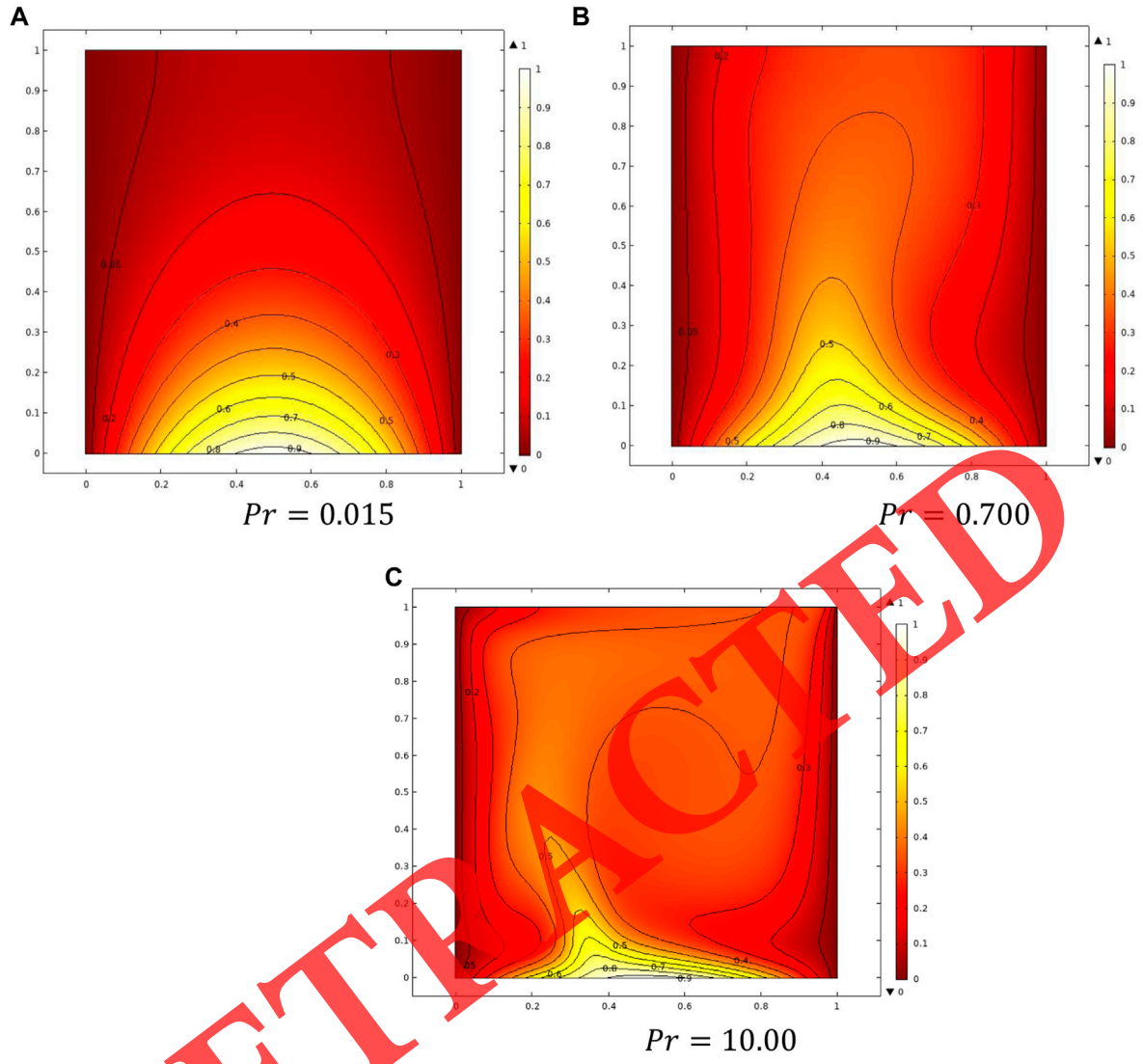

FIGURE 16
Influence of *Pr* on temperature distribution for the non-uniform heating case: **(A)** $Pr = 0.015$, **(B)** $Pr = 0.700$, and **(C)** $Pr = 10.00$.

Figures 16A–C. An increment in *Pr* tends to produce more heat flux in the domain as an outcome of temperature profile upsurge. In addition, it is because of the reason that by increasing *Pr*, momentum diffusivity rises due to which the average kinetic energy mounts and causes a positive effect on temperature. It is worthwhile to mention that in the case of non-uniform heating, thermal discontinuity is removed.

The measurement of the heat flux coefficient against the Reynolds number (*Re*) for n = 0.8, 1, and 1.2 and Pr = 0.015 and 10 is discussed in Figure 17. It is seen that for all magnitudes of *Re* and for $n = 1.2$, no significant change in heat flux is attained, whereas at $Re > 10$ and for $n = 1$, elevation in heat flux is found. The reason behind this behavior is that by increasing *Re*, viscosity of the fluid decreases due to which the kinetic energy of molecules lifts and the associated heat energy also elevates.

Plotting of the average Nusselt number against *Re* for $n < 1$ and $n > 1$ along with fixation of $Pr = 0.015$ and 10 is displayed in Figure 18. It is observed that the heat flux coefficient in the case of $n = 1$ is more than that for shear thickening situation ($n > 1$). In addition, it is seen that for all values of *n*, the average Nusselt number intensifies against *Re*.

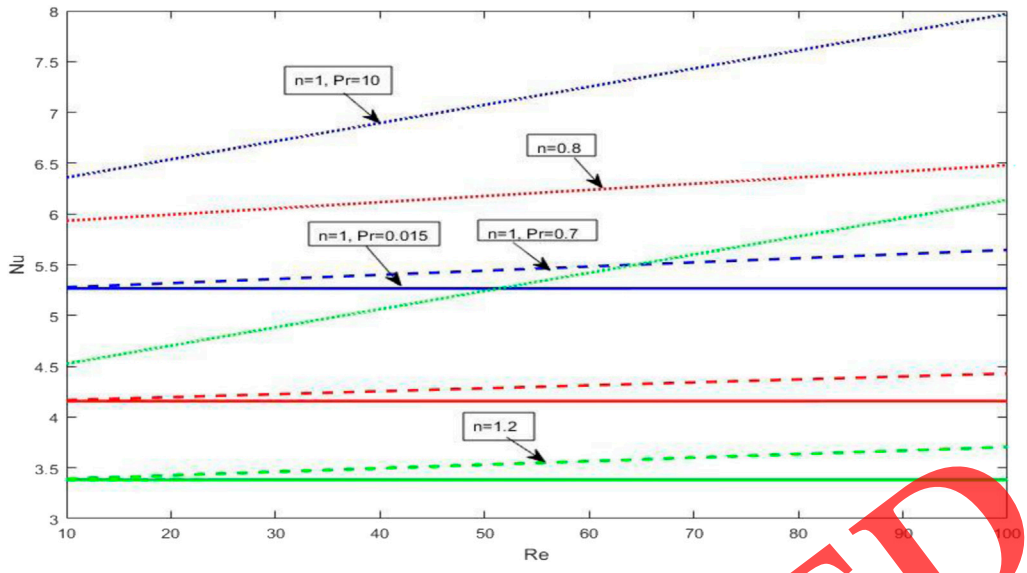

FIGURE 17
Variation in the local Nusselt number (Nu_{Local}) against the Reynolds number (Re).

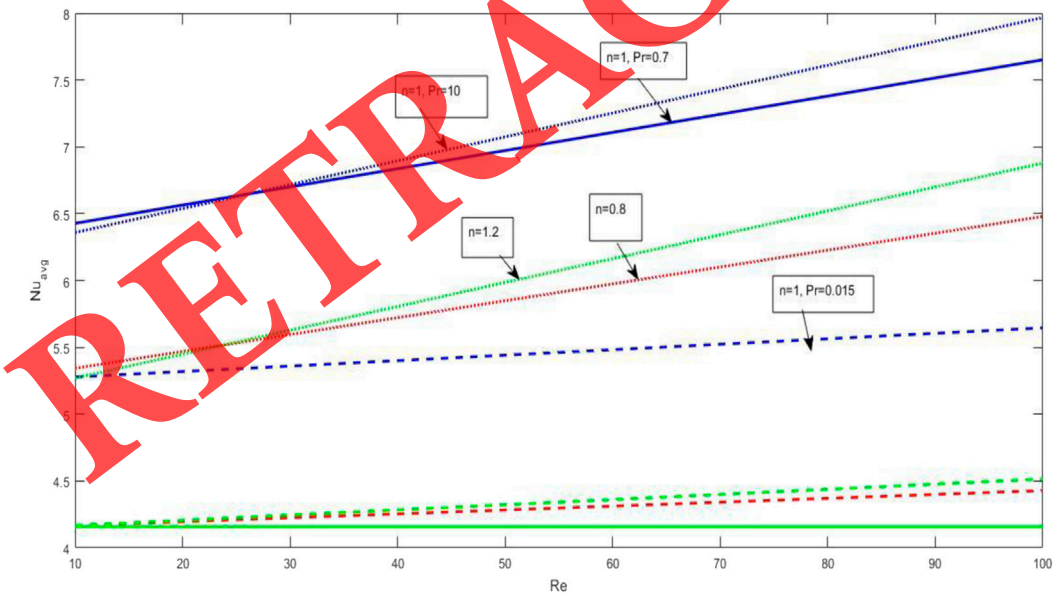

FIGURE 18
Variation in the average Nusselt number (Nu_{Avg}) against the Reynolds number (Re).

Variation in the kinetic energy along the vertical cutline against Re is shown in Figure 19 for each case of n. When we increase the value of (Re) from 1 to 100, we can observe that $K.E$ increases abruptly. It is due to the fact that an increment in the Reynolds number (Re) causes the viscosity to reduce, and as a result, the energy due to the motion of fluid increases gradually.

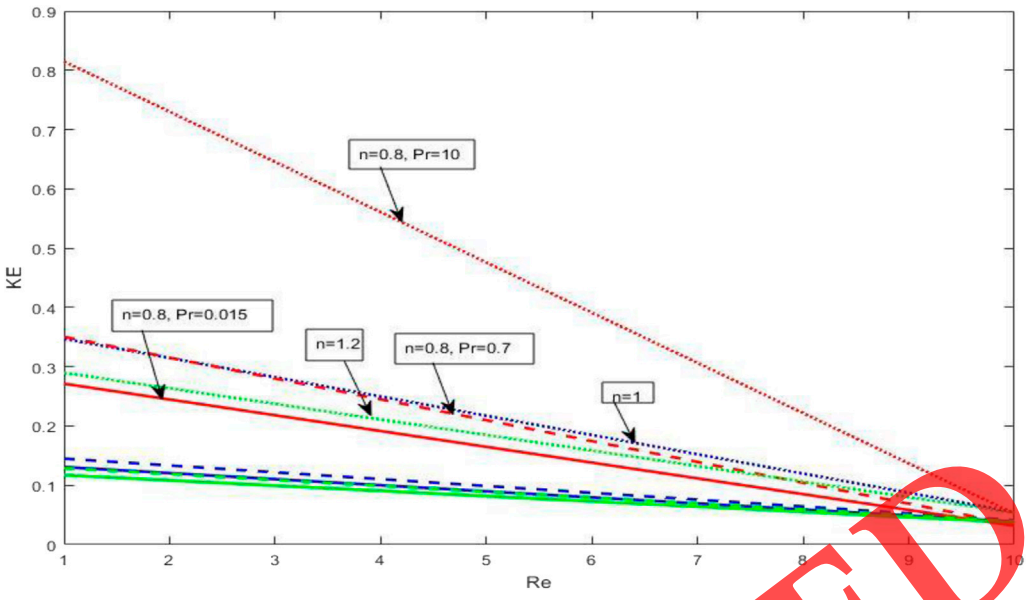

FIGURE 19
Variation in the kinetic energy (*K.E*) against the Reynolds number (*Re*).

5 Conclusion

In this article, the authors have dedicated their efforts to investigate hydrothermal attributes of the power-law liquid in a square enclosure by incorporating the aspects of inertial and buoyancy forces. The formulation of the problem conceding the aspects of mixed convection in the non-Newtonian model is attained in the form of complex PDEs. Finite element computations are performed to resolve the coupled system of equations. The results are drawn in a graphical manner to disclose the impact of flow concerning parameters. Some key findings are itemized as follows:

1) Thermal singularity is removed in the case of non-uniform heating and retained in uniform heating.
2) At $Re = 1$, the inertial forces and buoyancy forces balance each other, whereas in the case of $Re = 100$, forced convection dominates over natural convection.
3) The local and global heat flux coefficient increases against uplift in *Re*.
4) The kinetic energy of the fluid depreciated against *Re*.
5) At a low magnitude of *Pr*, no significant effect of *Re* on the temperature distribution is seen in both cases.
6) In the case of a high Prandtl number (*Pr*), the movement of the fluid squeezes due to the uplift in the viscous diffusion.

Data availability statement

The original contributions presented in the study are included in the article/supplementary material, Further inquiries can be directed to the corresponding author.

Author contributions

All authors listed have made a substantial, direct, and intellectual contribution to the work and approved it for publication.

Acknowledgments

The authors would like to thank the Deanship of Scientific Research at Umm Al-Qura University for supporting this work by Grant Code: (22UQU4282396DSR30) (sehazmi@uqu.edu.sa).

Conflict of interest

The authors declare that the research was conducted in the absence of any commercial or financial relationships that could be construed as a potential conflict of interest.

Publisher's note

References

1. Lyican L, Bayazitoglu Y. An analytical study of natural convective heat transfer within trapezoidal enclosure. *ASME Trans J Heat Transf* (1980) 102:640–7. doi:10.1115/1.3244365

2. Roy S, Basak T. Finite element analysis of natural convection flows in a square cavity with non- uniformly heated wall(s). *Int J Eng Sci* (2005) 45:668–80. doi:10.1016/j.ijengsci.2005.01.002

3. Amiri AM, Khanafer K, Pop I. Effect of sinusoidal wavy bottom surface on mixed convection heat transfer in a lid driven cavity. *Int J Heat Mass Transf* (2007) 50:1771–80. doi:10.1016/j.ijheatmasstransfer.2006.10.008

4. Varol Y, Oztop HF, Pop I. Numerical analysis of natural convection in an inclined trapezoidal enclosure filled with a porous medium. *Int J Therm Sci* (2008) 47:1316–31. doi:10.1016/j.ijthermalsci.2007.10.018

5. Varol Y, Oztop HF, Pop I. Natural convection in right-angle porous trapezoidal enclosure partially cooled from inclined wall. *Int Commun Heat Mass Transfer* (2009) 36:6–15. doi:10.1016/j.icheatmasstransfer.2008.09.010

6. Basak T, Roy S, Sharma PK, Pop I. Analysis of mixed convection flows within a square cavity with uniform and non-uniform heating of bottom wall. *Int J Therm Sci* (2009) 48:891–912. doi:10.1016/j.ijthermalsci.2008.08.003

7. Basak T, Roy S, Pop I. Heat flow analysis for natural convection within trapezoidal enclosures based on heat line concept. *Int J Heat Mass Transf* (2009) 52:2471–83. doi:10.1016/j.ijheatmasstransfer.2009.01.020

8. Oztop HF, Nada EA, Varoland Y, Chamkha AJ. Natural convection in wavy enclosures with volumetric heat sources. *Int J Therm Sci* (2011) 50:502–14. doi:10.1016/j.ijthermalsci.2010.10.015

9. Mahmoodi M, Talea'pour Z. Magnetohydrodynamic free convection heat transfer in a square enclosure heated from side and cooled from the ceiling. *Comput Therm Scien* (2011) 3:219–26. doi:10.1615/computthermalscien.2011002689

10. Rahman MM, Oztop HF, Saidur R, Mekhilef S, Salem KS. Unsteady mixed convection in a porous media filled lid-driven cavity heated by a semi-circular heaters. *Therm Sci* (2015) 19:1761–8. doi:10.2298/tsci130725098r

11. Jagadeesha RD, Prasanna BMR, Younghae D, Sankar M. Natural convection in an inclined parallelogrammic porous enclosure under the effect of magnetic field. *J Phys : Conf Ser* (2017) 908:012076. doi:10.1088/1742-6596/908/1/012076

12. Jagadeesha RD, Prasanna BMR, Sankar M. Numerical simulation of double diffusive magnetoconvection in an inclined parallelogrammic porous enclosure with an internal heat source. *Mater Today Proc* (2017) 4:10544–8. doi:10.1016/j.matpr.2017.06.417

13. Sankar M, Kiran S, Younghae D. Effect of nonuniform heating on natural convection in a vertical porous annulus. Flow and Transp. *Subsurface Environ* (2018) 17:251–78.

14. Sankar M, Kiran S, Sivasankaran S. Natural convection in a linearly heated vertical porous annulus. *J Phys : Conf Ser* (2018) 1139:012018. doi:10.1088/1742-6596/1139/1/012018

15. Kiran S, Sankar M, Gangadharaiah YH, Dhananjayamurthy BV. Natural convection in a linearly heated vertical porous annulus under the effect of magnetic field. *Adv Mech Engg* (2021) 22:537–46.

16. Sankar M, Kiran S, Ramesh GK, Makinde OD. Natural convection in a non-uniformly heated vertical annular cavity. *Defect and Diffusion Forum* (2017) 377:189–99. doi:10.4028/www.scientific.net/ddf.377.189

17. Hartnett MLN, Hartnett J. Natural convection in power-law fluids. *Int Commun Heat Mass Transfer* (1986) 13:115–20. doi:10.1016/0735-1933(86)90078-3

18. Khezzar L, Siginer D, Vinogradov I. Natural convection of power law fluids in inclined cavities. *Int J Therm Sci* (2012) 53:8–17. doi:10.1016/j.ijthermalsci.2011.10.020

19. Sairamu M, Chhabara RP. Natural convection in power-law fluids from a tilted square in an enclosure. *Int J Heat Mass Transf* (2013) 56:319–39. doi:10.1016/j.ijheatmasstransfer.2012.09.033

20. Mishra L, Chhabra RP. Natural convection in power-law fluids in a square enclosure from two differentially heated horizontal cylinders. *Heat Transf Engg* (2018) 38:319–42.

21. Wakif A, Shah NA. *Hydrothermal and mass impacts of azimuthal and transverse components of Lorentz forces on reacting Von Kármán nanofluid flows considering zero mass flux and convective heating conditions*. London: Waves in Random and Complex Media (2022). p. 1–22.

22. Subray A, Hanumagowda PVBN, Varma SVK, Zidan AM, Alaoui MK, Raju CS, et al. Dynamics of heat transfer analysis of convective-radiative fins with variable thermal conductivity and heat generation: Differential transformation method. *Mathematics* (2022) 10:3814. doi:10.3390/math10203814

23. Vieru D, Fetecau C, Shah NA, Yook S-J. Unsteady natural convection flow due to fractional thermal transport and symmetric heat source/sink. *Alexandria Eng J* (2022). doi:10.1016/j.aej.2022.09.027

24. Ramesh GK, Madhukesh JK, Shah NA, Yook S-J. Flow of hybrid CNTs past a rotating sphere subjected to thermal radiation and thermophoretic particle deposition. *Alexandria Eng J* (2022). doi:10.1016/j.aej.2022.09.026

25. Rasool G, Shah NA, El-Zahar ER, Wakif A. *Numerical investigation of EMHD nanofluid flows over a convectively heated riga pattern positioned horizontally in a Darcy-forchheimer porous medium: Application of passive control strategy and generalized transfer laws*. London: Waves in Random and Complex Media (2022). p. 1–20.

26. Ogami Y. Simulation of hat fluid motion by the vortex method. *J.S.M.E Int J* (2001) 44:513–9. doi:10.1299/jsmeb.44.513

27. Moraes PG, Oliveira MA, Bimbato AL, Pereira LAA. A Lagrangian description of buoyancy effects on aircraft wake vortices from wing tips near a heated ground plane. *Energies* (2012) 15:6995. doi:10.3390/en15196995)

28. Abualnaja KM. An innovative way to generate Hamiltonian energy of a new hyperchaotic complex nonlinear model and its control. *Complexity* (2020) 2020:1–10. doi:10.1155/2020/6690955

29. Ahsan S, Nawaz R, Akbar M, Nisar KS, Abualnaja KM, Mahmoud EE, et al. Numerical solution of two-dimensional fractional order Volterra integro-differential equations. *AIP Adv* (2021) 11(3):035232. doi:10.1063/5.0032636